CHEMISTRY
A EUROPEAN JOURNAL

DOI: 10.1002/chem.201201793

Photophysical Analysis of 1,10-Phenanthroline-Embedded Porphyrin Analogues and Their Magnesium(II) Complexes

Masatoshi Ishida,[a, b] Jong Min Lim,[b] Byung Sun Lee,[b] Fumito Tani,[a] Jonathan L. Sessler,*[b, c] Dongho Kim,*[b] and Yoshinori Naruta*[a, d]

Abstract: The synthesis, characterization, photophysical properties, and theoretical analysis of a series of tetraaza porphyrin analogues (**H−P*n***: $n=1$–4) containing a dipyrrin subunit and an embedded 1,10-phenanthroline subunit are described. The *meso*-phenyl-substituted derivative (**H−P1**) interacts with a Mg^{2+} salt (e.g., $MgCl_2$, $MgBr_2$, MgI_2, $Mg(ClO_4)_2$, and $Mg(OAc)_2$) in MeCN solution, thereby giving rise to a cation-dependent red-shift in both the absorbance- and emission maxima. In this system, as well as in the other **H−P*n*** porphyrin analogues used in this study, the four nitrogen atoms of the ligand interact with the bound magnesium cation to form Mg^{2+}–dipyrrin–phenanthroline complexes of the general structure **MgX−P*n*** (X = counteranion). Both single-crystal X-ray diffraction analysis of the corresponding zinc-chloride derivative (**ZnCl−P1**) and fluorescence spectroscopy of the Mg-adducts that are formed from various metal salts provide support for the conclusion that, in complexes such as **MgCl−P1**, a distorted square-pyramidal geometry persists about the metal cation wherein a chloride anion acts as an axial counteranion. Several analogues (**H−P*n***) that contain electron-donating and/or electron-withdrawing dipyrrin moieties were prepared in an effort to understand the structure–property relationships and the photophysical attributes of these Mg–dipyrrin complexes. Analysis of various **MgX−P*n*** (X = anion) systems revealed significant substitution effects on their chemical, electrochemical, and photophysical properties, as well as on the Mg^{2+}-cation affinities. The fluorescence properties of **MgCl−P*n*** reflected the effect of donor-excited photoinduced electron transfer (d-PET) processes from the dipyrrin subunit (as a donor site) to the 1,10-phenanthroline acceptor subunit. The proposed d-PET process was analyzed by electron paramagnetic resonance (EPR) spectroscopy and by femtosecond transient absorption (TA) spectroscopy, as well as by theoretical DFT calculations. Taken together, these studies provide support for the suggestion that a radical species is produced as the result of an intramolecular charge-transfer process, following photoexcitation. These photophysical effects, combined with a mixed dipyrrin–phenanthroline structure that is capable of effective Mg^{2+}-cation complexation, lead us to suggest that porphyrin-inspired systems, such as **H−P*n***, have a role to play as magnesium-cation sensors.

Keywords: electron transfer · fluorescent probes · magnesium · phenanthrolines · porphyrinoids

Introduction

Intracellular magnesium ions (as Mg^{2+}) play a number of critical roles in biological systems.[1] In normally functioning cells, Mg^{2+} ions are involved in energy metabolism, and a dietary deficiency of Mg^{2+} has been correlated with many neuronal diseases, including Alzheimer's disease, migraines, and Parkinson's disease.[2] This importance has provided an incentive to develop new chemosensors ("sensors") for Mg^{2+} ions because, ultimately, such probes could facilitate Mg^{2+} recognition and detection in vivo.[3] Among the limitations that are associated with many of the current Mg^{2+}-responsive fluorescent sensors is interference from the ubiquitous divalent calcium ion, Ca^{2+}. Furthermore, the emission wave-

---

[a] Dr. M. Ishida, Prof. Dr. F. Tani, Prof. Dr. Y. Naruta
Institute for Materials Chemistry and Engineering
Kyushu University, 6-10-1 Higashi-ku
Fukuoka, 812-8581 (Japan)
Fax: (+81) 92-642-2731
E-mail: naruta@ms.ifoc.kyushu-u.ac.jp

[b] Dr. M. Ishida, J. M. Lim, B. S. Lee, Prof. Dr. J. L. Sessler,
Prof. Dr. D. Kim
Department of Chemistry and Spectroscopy Laboratory for
Functional π-Electronic Systems, Yonsei University
262 Seongsanno Seodaemun-gu, Seoul 120-749 (Korea)
Fax: (+82) 2-2123-2434
E-mail: dongho@yonsei.ac.kr

[c] Prof. Dr. J. L. Sessler
Department of Chemistry and Biochemistry
The University of Texas at Austin
1 University Station - A5300, Austin, TX 78712-0165 (USA)
Fax: (+1) 512-471-5009
E-mail: sessler@cm.utexas.edu

[d] Prof. Dr. Y. Naruta
International Institute for Carbon-Neutral Energy
Research (WPI-I^{2}CNER), Kyushu University
6-10-1 Higashi-ku, Fukuoka, 812-8581 (Japan)

Supporting information for this article is available on the WWW under http://dx.doi.org/10.1002/chem.201201793.

length in most Mg^{2+}-responsive ratiometric fluorescent sensors falls below about 550 nm, which, in the final in vitro or in vivo applications, could lead to interference from endogenous fluorophores. Thus, there is a need for Mg^{2+} sensors that emit light at longer wavelengths.

Inspired by the chemical structure of Mg–chlorophylls present in the photosynthetic light-harvesting complex, we have recently designed porphyrin-related macrocycle **H−P1** and studied it as a Mg^{2+}-sensing unit (Scheme 1).[4] This porphyrin-based macrocycle was found to be effective for the detection of Mg^{2+} ions in aqueous DMSO, as well as in MeCN. It produces a relatively long-wavelength emission ($\lambda_{max} = 640$ nm) and displays good selectivity for Mg^{2+} ions over most physiologically important cations, including—notably—Ca^{2+}. Herein, we analyze in detail the photophysics and the underlying theoretical determinants of the Mg^{2+}-based response of **H−P1** and extend these studies to include several new analogues of this first-generation system.

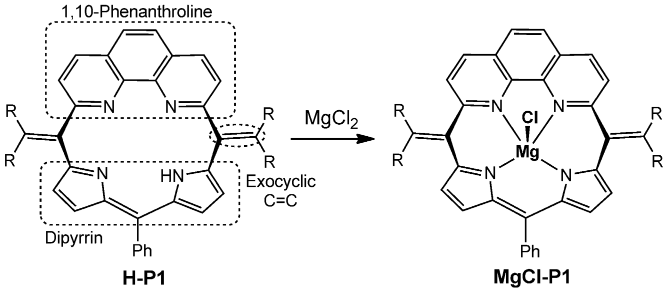

Scheme 1. Schematic representation of the core structure and key design features of Mg^{2+}-ion receptor **H−P1** ($R = CO_2Et$).

From a structural point of view, this heteroleptic dipyrrin–phenanthroline-hybrid ligand gives rise to a stable Mg–dipyrrin complex (**MgX−P1**: X = counteranion) when exposed to various magnesium salts. This Mg adduct is regarded as an analogue of the corresponding boron-difluoride–dipyrrin complexes, of which BODIPY (4,4-difluoro-4-bora-3a,4a-diaza-s-indacene) is the best known. This latter system is recognized for its high fluorescence, good chemical stability, and the fact that the wavelength of its emission maximum can be tuned through modification of the dipyrrin structure and through the choice of the coordinated cationic center.[5] In fact, many dipyrrin-based metal complexes have been explored for use in biological and materials applications.[6] A few dipyrrinato complexes with transition-metal cations, such as Zn,[7] Al,[8] Ga,[9] In,[9] Sn,[10] Si,[11] Pd,[12] Pt,[12] Rh,[13] and Ir,[14] display emissive character. However, to the best of our knowledge, no Mg–dipyrrin complex has been reported, presumably owing to the inherent chemical instability of stand-alone Mg^{2+}–dipyrrin complexes.[15] Thus, in our system, the heteroleptic macrocyclic core of **H−P1** allows us to investigate the structural and photophysical properties of Mg^{2+}–dipyrrin complexes.

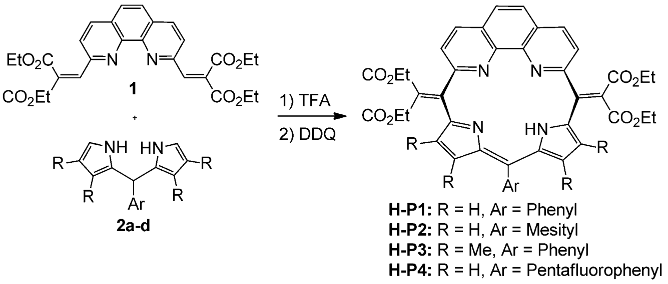

Scheme 2. Syntheses of **H−P*n*** ($n = 1$–4).

To assess the further effect of structural changes on the electronic features of the basic 1,10-phenanthroline-embedded porphyrin framework present in **H−P1**, we have prepared several new analogues, namely **H−P*n***: $n = 1$–4, and investigated their photophysical properties (Scheme 2). These compounds differ in the size and electronic character of their peripheral substituents and contain, respectively, *meso*-phenyl (**H−P1**), *meso*-mesityl (**H−P2**), *β*-tetramethyl (**H−P3**), and *meso*-pentafluorophenyl functionality (**H−P4**). These resulting structures allowed us to obtain basic insights into the nature of the macrocyclic core and, thus, provided a foundation for understanding the relationship between the structure and the associated chemical and photophysical properties of the corresponding Mg-adducts derived from a range of electron-rich to electron-deficient ligands. In accordance with design expectations, modification of the dipyrrin unit (the expected fluorophore in **H−P*n***) led to discernible differences in their fluorescent-emission efficiency, redox potentials, and cation-binding affinities. The observed structure-dependent changes in the photophysical properties were fully supported by theoretical DFT calculations. These changes are especially manifest in the luminescent character of the Mg-adducts (**MgCl−P*n***; $n = 1$–4), as reflected in the donor-excited photoinduced electron-transfer (d-PET) process, wherein the photoexcited dipyrrin and the ground-state 1,10-phenanthroline subunits act as donors and acceptors, respectively.

Results and Discussion

Ligand design for Mg^{2+}-ion binding: **H−P*n*** have several structural features that facilitate the complexation of Mg^{2+} ions, namely: 1) a non-planar macrocyclic geometry, 2) a single acidic proton that makes it a monoanionic ligand, and 3) a smaller coordination sphere (Scheme 1). According to theoretical analyses, the complexation of Mg^{2+} ions to porphyrins requires deformation of the porphyrin ring during the initial step. Then, the first bond between the metal center and one of the pyrrolic nitrogen atoms of the porphyrin ligand forms as the rate-limiting step on the pathway to metal complexation.[16] Consistent with this suggestion is the finding that distorted free-base porphyrins, including ones with bulky peripheral side-chains and substituents on

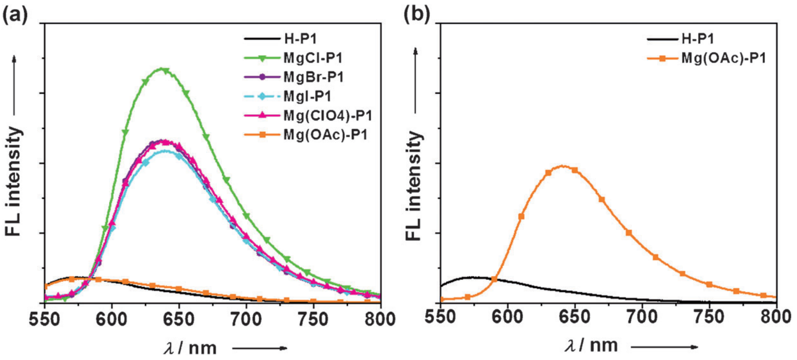

Figure 1. a) Fluorescence spectra of **H−P1** (2×10^{-5} M, black line) in the presence of various magnesium salts in MeCN: $MgCl_2$ (green), $MgBr_2$ (purple), MgI_2 (sky blue), $Mg(ClO_4)_2$ (pink), and $Mg(OAc)_2$ (orange). b) Fluorescence spectra of **H−P1** (black) in MeCN after standing for 24 h in the presence of $Mg(OAc)_2$ (orange); $\lambda_{ex}=520$ nm.

the macrocycle, exhibit metalation rates that are 10^3–10^5 times higher than those of their planar analogues.[17] Thus, the introduction of *exo*-alkylidenyl double bonds at the *meso* positions of the macrocycle is expected to stabilize a distorted gable-shaped coordination geometry, which, in turn, should open up the core to access by the incoming Mg^{2+} ion. We further considered that the replacement of a dipyrrin-like "porphyrin half" by a 1,10-phenanthroline unit bearing two aromatic nitrogen atoms would provide shorter nitrogen−nitrogen distances than are typical for porphyrins. In turn, we thought that this ligand would be useful for the coordination of the relatively small Mg^{2+} ion (ionic radius: 0.72 Å[18]). We were also cognizant of the fact that 1,10-phenanthroline has been used as an indicator for determining the concentration of Grignard reagents, thereby leading us to infer that, once embedded in a porphyrin-like macrocycle, it could stabilize a bound Mg^{2+} cation.[19] In fact, **H−P1** was found to be a highly effective ligand for Mg^{2+} ions.

Coordination geometry of the Mg^{2+} adduct, MgCl−P1: According to our previous findings, **H−P1** is capable of stabilizing the corresponding Mg adduct upon exposure to $MgCl_2$ in MeCN.[4] The coordination of a magnesium cation within the **H−P1** core was confirmed by optical and NMR spectroscopy, as well as by HRMS (FAB; see the Supporting Information, Figure S1). However, an inability to obtain diffraction-grade crystals (see above) precluded a direct elucidation of the coordination geometry within this complex by using X-ray diffraction analysis. Previously, a related system, the copper(II) complex of **H−P1**, was found to adopt a square-planar geometry with a non-coordinating hexafluorophosphate (PF_6^-) anion.[20] This result is consistent with the notion that the **H−P1** ligand can provide a monoanionic coordination environment for divalent cations. Thus, a square-pyramidal structure was expected for the corresponding adduct, **MgCl−P1**, wherein the chloride counteranion would serve as an axial ligand.

Support for the proposal that the counteranion would be ligated to the coordinated magnesium center in an axial fashion came from preliminary studies of complexes that were produced from the reactions of **H−P1** with various magnesium salts (e.g., $MgCl_2$, $MgBr_2$, MgI_2, $Mg(ClO_4)_2$, and $Mg(OAc)_2$) in MeCN under ambient conditions. With the exception of the acetate salt, the products were formed quickly on a preparative timescale and gave rise to similar levels of emission enhancement (i.e., the appearance of a feature at around 640 nm). This result is consistent with the magnesium complexes in question (i.e., **MgX−P1**; X = Cl, Br, I, ClO_4), which formed quickly with all of the tested magnesium salts except for the presumed acetate derivative, **Mg(OAc)−P1** (Figure 1). In the case of $Mg(OAc)_2$, the rate of complexation was slow. However, allowing a mixture of **H−P1** and $Mg(OAc)_2$ in MeCN to stand for more than 24 h at room temperature led to the formation of the expected magnesium acetate complex, as evidenced by an increased emission intensity at 639 nm.[21] Importantly, the emission properties of **MgX−P1** were dependent upon the properties of the Mg salts that contained different counteranions. The emission intensities of the Mg adducts of the bromide and iodide derivatives (**MgBr−P1** and **MgI−P1**, respectively) decreased relative to those of the chloride derivative (**MgCl−P1**). Presumably, this decrease reflects an intramolecular heavy-atom effect that serves to diminish the efficiency of the fluorescence emission. However, the fact that an anion-dependence of the emission behavior was observed provides support for the basic structural inference that each **MgX−P1** complex contains an axially ligated counteranion that is bound to the Mg^{2+} center. This result was also expected to be true for the corresponding species that were derived from other ligands, namely **MgX−P*n***, where $n=2$–4 (see below).

To obtain further insight into the geometry of the Mg adducts of **H−P*n*** and to confirm the basic ligand structure, an effort was made to characterize structurally an analogous metal complex. Based on the expected analogy in coordination environments with those in various crystallographically characterized complexes of monoanionic porphyrin analogues with zinc(II) chloride,[22] the zinc(II) chloride complex (**ZnCl−P1**) of **H−P1** was considered as a promising structural "surrogate". Complex **ZnCl−P1** was prepared by treating **H−P1** with zinc(II) chloride in $CHCl_3$/MeOH (5:1) in the presence of 2,6-lutidine. Single crystals of **ZnCl−P1** that were suitable for X-ray diffraction were obtained by the slow evaporation of a $CHCl_3$/MeOH mixture.

The crystal structure of **ZnCl−P1**[23] revealed that the zinc center is pentacoordinate and adopts a distorted square-pyramidal geometry wherein the macrocyclic ligand provides

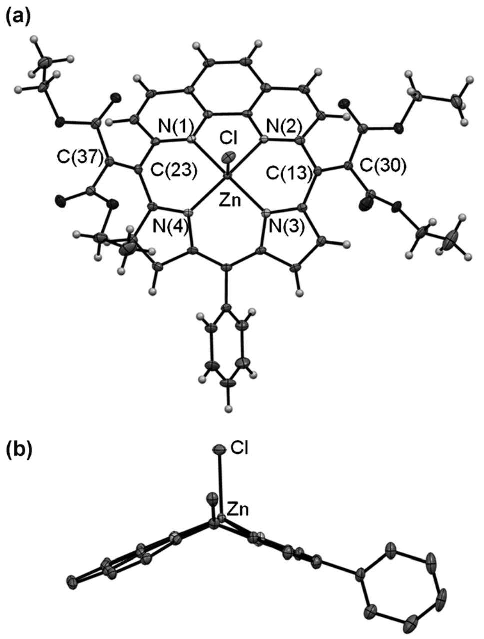

Figure 2. ORTEP of a) **ZnCl−P1·CHCl$_3$**; ellipsoids are set at the 50 % probability level. The hydrogen atoms, ethyl ester groups, and solvate molecules have been omitted for clarity in (b). Selected bond lengths [Å] and angles [°]: Zn–N(1) 2.161(1), Zn–N(2) 2.167(1), Zn–N(3) 2.046(1), Zn–N(4) 2.031(1), Zn–Cl 2.2503(5), C(13)–C(30) 1.346(3), C(23)–C(37) 1.354(3); N(1)-Zn-N(2) 76.39(5), N(2)-Zn-N(3) 83.68(5), N(3)-Zn-N(4) 85.15(6), N(4)-Zn-N(1) 90.04(6), N(1)-Zn-N(3) 138.91(6), N(2)-Zn-N(4) 142.98(6).

four equatorial nitrogen atoms and the fifth ligand consists of a chloride counteranion that is bound in an axial manner (Figure 2). The metal ion is located about 0.688 Å above the mean plane that is defined by the four nitrogen atoms. The Zn−N(1) and Zn−N(2) bond lengths (2.16–2.17 Å) are longer than those of the Zn−N(3) and Zn−N(4) bonds (2.03–2.04 Å), in analogy to what was found for the corresponding copper(II) complex.[20] This asymmetric positioning of the zinc center within the central cavity leads us to consider that the extent of ligation differs between the neutral 1,10-phenanthroline donor and the monoanionic *meso*-phenyldipyrrin subunit, with the latter unit being more important in terms of stabilizing complex formation. Such a conclusion is consistent with the zinc(II) chloride complex of pyriporphyrin, wherein an unsymmetrical coordination environment was found (Zn−N$_{\text{pyridine}}$: 2.353 Å, Zn−N$_{\text{pyrrole}}$: 2.05–2.11 Å), albeit with a larger displacement from the mean plane (0.512 Å).[21b]

The macrocycle framework of **ZnCl−P1** adopts a nonplanar gable conformation, based on the dihedral angle between the 1,10-phenanthroline plane and that defined by the dipyrromethene subunit (about 117°). This angle is slightly smaller than that of the free-base **H−P1** (122–124°).[4] Importantly, the optimized structure of **MgCl−P1** obtained from calculations at the B3LYP/6-31G(d) level is also gable-like and is characterized by an unsymmetric binding environment for the Mg^{2+} cation. Thus, the calculated structure reproduces well the experimentally derived X-ray structure of **ZnCl−P1** (see above and the Supporting Information, Figure S2).

Substitution effects on photophysical properties and binding affinities: The exposure of **H−P1** to MgCl$_2$ gives rise to an intense band at around 640 nm in the emission spectrum (see the Supporting Information, Figure S2). Whereas the overall emission efficiency ($\Phi_{\text{fl}} = 0.015$) of the corresponding **MgCl−P1** complex is low, these optical changes could provide a ratiometric basis for Mg^{2+}-ion detection. To explore this possibility, additional modified macrocycles that are analogous to **H−P1** were designed and synthesized. These new systems, **H−P*n*** ($n = 2$–4; Scheme 2), incorporate peripheral substituents at either the *meso* or β-pyrrolic positions of the dipyrrin.

The choice of specific **H−P*n*** ($n = 2$–4) targets was based on the expectation—supported by DFT calculations—that the photophysical properties of this general class of porphyrin analogue would largely be dominated by the dipyrrin moiety. In designing each particular derivative, the following previous findings were considered: First, we recognized that the presence of methyl groups at the *ortho* positions on a *meso*-aryl ring in BODIPYs[10] or in dipyrrinato metal complexes (M = Al, Zn, Ga, In, Sn)[11–15] gives rise to a distinct increase in fluorescent quantum yield, as does the presence of methyl groups on the adjacent β-pyrrolic positions. Presumably, this increase reflects the restricted rotation of the *meso*-aryl ring relative to the core plane of the dipyrrin chromophore. In fact, enhanced emission has also been seen in *meso*-2-pyridyl dipyrrin complexes as the result of metal-based restrictions in rotation.[11e] Second, we appreciated that other physicochemical properties, such as the stability of the complex, the extent of supramolecular association, and the inherent cation-binding capability, would also be dependent on the specific structures of the macrocycles.[24] On this basis, the *meso*-mesityl- (**H−P2**) and β-tetramethyl-substituted systems (**H−P3**) were designed and prepared. Third, we noted that an enhanced emission intensity is seen in peripheral-fluorinated magnesium porphyrins, likely as the result of a shift in electron density from the macrocycle and the metal onto the fluorinated phenyl rings.[25] Given this precedent, *meso*-pentafluorophenyl substituents were introduced as putative electron-withdrawing groups in the case of target **H−P4**; thus, this latter system was expected to provide an electron-deficient complement to the electron-rich targets (**H−P2** and **H−P3**).

The new members of the **H−P*n*** series were prepared in analogy to the approach that was used to prepare **H−P1**. Thus, McDonald [2+2]-type condensations were carried out between 1,10-phenathroline vinyl ester **1** and the corresponding aryl-dipyrromethanes (**2b**–**2d**; Scheme 2). The resulting macrocyclic products were characterized by ^{1}H NMR, ^{13}C NMR, and ^{19}F NMR spectroscopy, HRMS, and elemental analysis. Upon addition of MgCl$_2$ into solutions of **H−P*n*** in MeCN, complexation of the Mg^{2+} cation occurred, as inferred from the observation of the expected mass values in the mass spectra (MALDI-TOF), namely *m/z* 801.94, 815.05, and 849.87 for [**Mg−P2**]$^+$, [**Mg−P3**]$^+$, and [**Mg−P4**]$^+$, respectively. Features in the optical spectra (UV/Vis absorption and fluorescence) that were consistent with what would be expected for these complexes were also observed, as discussed below.

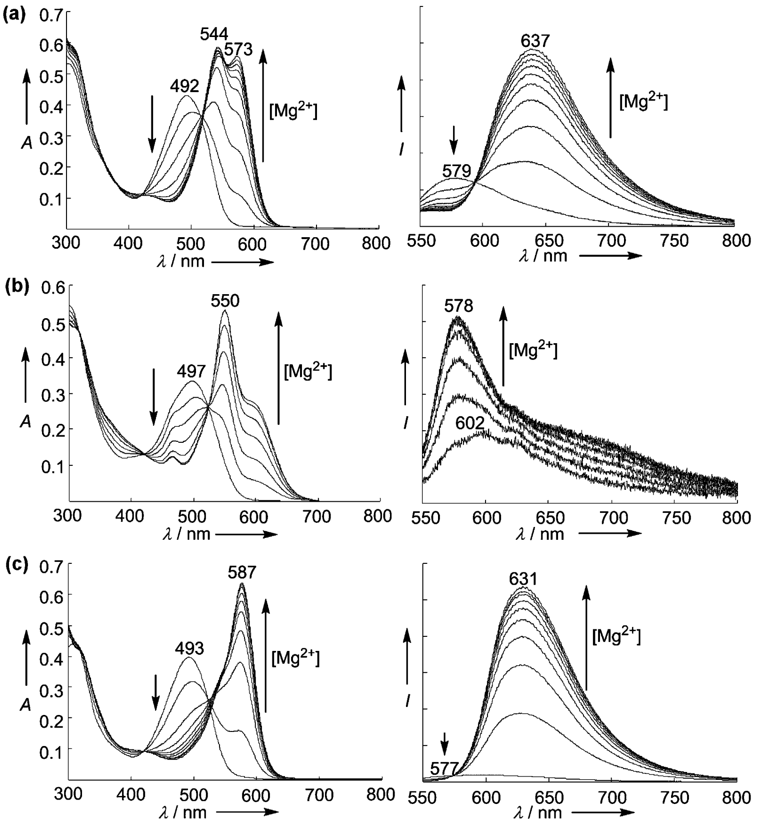

Figure 3. Changes in the absorption- (left) and emission spectra (right) of a) **H−P2**, b) **H−P3**, and c) **H−P4** in MeCN upon titration with $MgCl_2$. For the fluorescence-emission studies, a λ_{ex} value was used that corresponded to the isosbestic point in the absorption spectra upon the addition of a Mg^{2+} salt.

Two sterically restricted derivatives, **H−P2** (bearing a mesityl group at the *meso* position) and **H−P3** (bearing four methyl groups at the β-pyrrolic positions), were tested for their ability to act as colorimetric and fluorescent sensors for Mg^{2+} ions, in accord with the procedures that were used for **H−P1** (Figure 3 a–d). With both derivatives, the addition of Mg^{2+} ions gives rise to red-shifts in the absorption peaks and an increase in their spectroscopic intensities relative to **H−P1**. However, the fluorescence quantum yield was modest in the case of **MgCl−P2** ($\Phi_{fl} = 0.013$) with almost no emission intensity seen for **MgCl−P3** ($\Phi_{fl} < 0.001$; Table 1).[26]

The electron-deficient derivative **H−P4**, bearing a pentafluorophenyl group at the central *meso* position, was also tested. In sharp contrast to the electron-rich derivatives **H−P2** and **H−P3**, titration with $MgCl_2$ gave rise to a large increase in the fluorescent emission ($\Phi_{fl} = 0.078$; cf. Figure 3 e,f and Table 1). The fluorescence-enhancement factor (FEF) of about 39 seen upon formation of the associated Mg^{2+} complex (**MgCl−P4**) is significantly larger than that of the other derivatives. Because such a dramatic enhancement is not observed for **H−P3** (which bears a *meso*-phenyl substituent) upon conversion into its corresponding Mg^{2+} complex, this enhancement is not thought to reflect a steric effect. Rather, this effect is ascribed to the specific electronic structure of the macrocycle in question (i.e., acceptor versus donor *meso* substituents).

As can be seen from an analysis of the K_{Mg} values (Table 1 and the Supporting Information, Figure S3) the Mg^{2+}-cation-binding affinities for **H−Pn** decrease according to the sequence **H−P3** > **H−P2** > **H−P1** > **H−P4**, in accord with the expected inductive effects. For instance, derivative **H−P3**, which directly incorporates electron-donating β-methyl groups, was found to complex Mg^{2+} ions most effectively. In contrast, the corresponding K_{Mg} value for **H−P4**, whose electronic properties are reversed, was found to be low (Table 1).

Table 1. Summary of the photophysical data of **H−P*n*** in MeCN.

Compounds	**H−P1**	**H−P2**	**H−P3**	**H−P4**
λ_{abs}(H) [nm][a]	489	492	497	493
λ_{em} (H) [nm][a]	572	579	602	587
λ_{abs} (Mg) [nm][a]	532, 565	544, 573	550	577
λ_{em} (Mg) [nm][a]	639	637	578	631
K_{Mg} [M^{-1}][b]	3.12×10^5	1.27×10^6	2.20×10^6	2.74×10^4
Φ_H[c]	0.003	0.002	> 0.001	0.002
Φ_{Mg}[c]	0.015	0.013	0.001	0.078
FEF[d]	5.0	6.5	1.3[h]	39.0
τ_e (H) [ps][e]	5.0	8.5	4.2	9.2
τ_e (Mg) [ps][e]	5.8(20), 182(80)	7.0(10), 195(90)	26	29(24), 578(76)
τ_{fl} (Mg) [ps][f]	252	270	n.d.[g]	721

[a] These values are for the peaks in the visible-light region; H = free base, Mg = MgCl complex. [b] The binding constants for Mg^{2+} ions were estimated by using nonlinear least-square analysis based on the absorption spectra of **H−P*n***. [c] Quantum yields were determined relative to tetraphenylporphyrin ($\Phi_{fl} = 0.065$), which was used as a reference. These values are subject to ±10% experimental error. [d] Fluorescence enhancement factor (FEF) between the free base and the Mg complex in solution, based on the respective quantum yields. [e] Time constants of the singlet excited state were obtained from a multiexponential global analysis of the relevant TA spectra; values in parentheses are percentages of the total amplitude. [f] Fluorescence lifetime; $\lambda_{ex} = 400$ nm. [g] Not determined. [h] Estimated based on a comparison of the relevant fluorescent intensities.

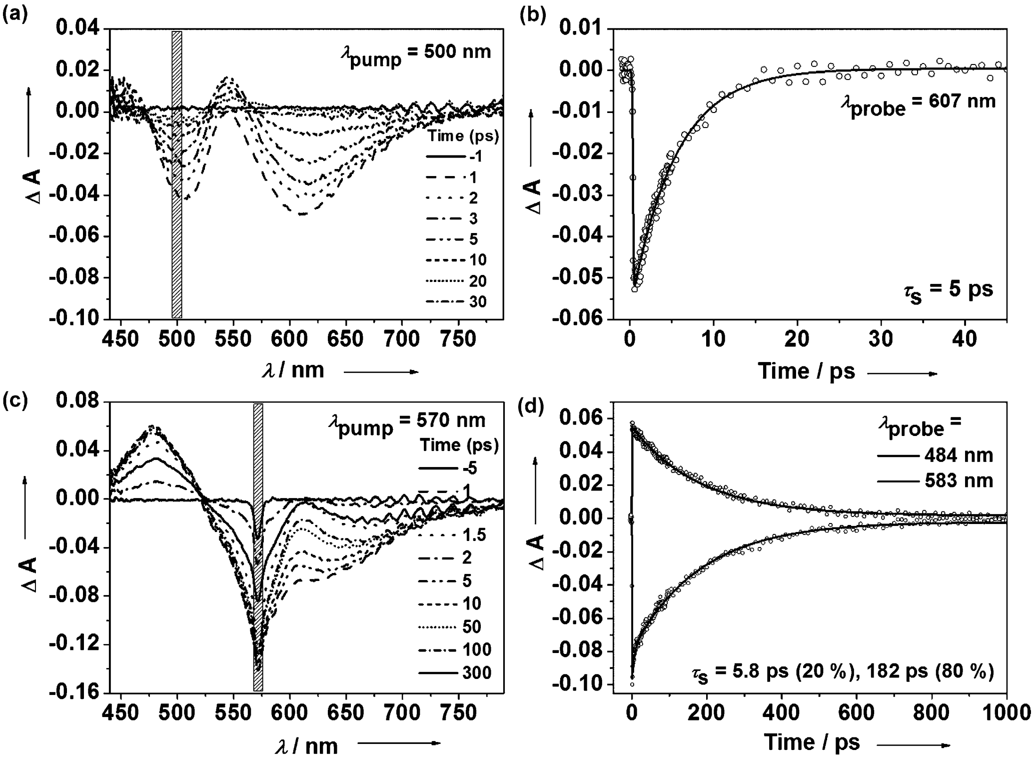

Figure 4. Femtosecond transient-absorption (TA) spectra of a) **H−P1** and c) **MgCl−P1** in MeCN at various decay times after excitation at 500 and 570 nm, respectively. The TA-decay profiles of b) **H−P1** at 607 nm and d) **MgCl−P1** at 484 and 583 nm, respectively.

In the optimized structures of **MgCl−P*n*** (all derived at the same calculation level), there is no significant difference between the derived structures; a similar distorted square-pyramidal geometry with an axial chloride anion was inferred in all cases (see the Supporting Information, Figure S2). In carrying out a detailed analysis of the bond lengths in the set of **MgCl−P*n*** complexes that were considered in this study, small changes in the Mg−N distances and the N-Mg-N angles were noted (see the Supporting Information, Table S1). For instance, **H−P3** showed a shorter distance between the nitrogen atoms of the dipyrrin moiety (N(3) and N(4)) and the central magnesium atom than the other derivatives. This result is consistent with the underlying hypothesis that electronic modulation of the dipyrrin subunit within the overall macrocyclic framework can be used to tune the binding affinities (and stabilities) of the corresponding Mg^{2+} complexes.

Time-resolved spectroscopy: In the steady-state optical spectra of **H−P*n*** and their Mg adducts, the electron-donating derivatives display relatively lower fluorescence quantum yields (see above); in contrast, the presence of electron-withdrawing groups serves to enhance the emission efficiency. To obtain further insight into the excited-state dynamics of these derivatives, femtosecond transient-absorption (TA) measurements were performed on the free-base ligands (**H−P*n***) and on their Mg adducts (**MgCl−P*n***) in MeCN at room temperature. Compared with the steady-state absorption and fluorescence spectra, the TA spectra of **H−P1** comprise two negative bands that are centered at $\lambda_{max}=510$ and 610 nm, respectively (Figure 4 and the Supporting Information, Figure S4); the former band can be ascribed to ground-state bleaching (GSB) and the latter band to the $S_1 \rightarrow S_0$ stimulated emission (SE). These TA spectroscopic features of **H−P1** are in line with most BODIPY-based complexes.[27]

The TA-decay profile of **H−P1** at 607 nm was fitted to a single exponential decay with a lifetime (τ_e) of 5 ps. This fast decay time is in agreement with its low quantum yield (Figure 4b). Consequently, the decay of photoexcited **H−P1** in MeCN is thought to occur predominantly through an $S_1 \rightarrow S_0$ nonradiative internal-conversion process. The decay profiles of all of the **H−P*n*** derivatives with lifetimes of less than 10 ps reflect the non-emissive properties that were observed in all of the free-base forms (cf. Figures S5–S7 in the Supporting Information). The TA spectroscopic features of **H−P*n*** are also quantitatively similar to those of **H−P1** and to one another, except for **H−P3** (see below).

Taking into account the thermodynamics, electron transfer from the dipyrrin subunit to the 1,10-phenanthroline moiety was expected to be favorable, based on an analysis of the respective Gibbs energies as inferred from the relevant optical- and electrochemical data (see below). Nevertheless, the TA spectra showed no clear feature that was attributable to the formation of a dipyrrin-radical cation. Whilst further analysis is required, this result could reflect the fact that the putative positive TA features of the dipyrrin-radical-cation species are masked by the strongly negative SE signals.

The UV/Vis spectrum of the one-electron-oxidation product of **H−P1** prepared electrochemically revealed a band at 529 nm with a broad tail to 800 nm; this band was red-shifted compared to that of the neutral ligand ($\lambda_{max} = 489$ nm; see the Supporting Information, Figure S7a). These red-shifted spectroscopic features were also observed in one-electron-oxidized BODIPY derivatives and, thus, are ascribed to the formation of the radical cation of the dipyrrin subunit that is present in **H−P1**.[28] The slightly intense positive signal in the spectroscopic window between the ground-state bleaching (GSB) and the SE features after a time delay of 5 ps may reflect an intramolecular charge-separation process that occurs in the excited state of **H−P1**, as has been observed in donor–acceptor BODIPY–dyad systems.[27–29] An alternative assignment, namely ascribing the signal between the GSB and SE bands to an excited-state-absorption (ESA) feature, can be discounted because the shape of the TA band is reasonably close to the spectrum of the one-electron-oxidized form of **H−P1** (see above).

This intermediate energy band becomes more pronounced in the **H−P3** derivative, which contains β-electron donor sites, presumably owing to poorer overlap with the SE band. The strong positive band that is centered at 565 nm with an associated tail in the NIR region (about 800 nm) in the TA spectra of **H−P3** provides further support for the assignment of this feature as a charge-separated state (see above). Moreover, the production of such a charge-separated state would account for the lack of emissive character in **H−P3** (see the Supporting Information, Figure S6).

The TA features of the magnesium complex, **MgCl−P1**, were also measured. This species gives rise to TA spectra that are characterized by a positive band centered at 480 nm, a GSB signal at 570 nm, and an SE band centered at around 640 nm (Figure 4c). Despite what are expected to be favorable energetics for electron transfer, a clear band ascribed to the radical cation of the Mg–dipyrrin chromophore was not clearly observed in the TA spectra.[30] The contribution of the putative Mg–dipyrrin cation radical might be small, perhaps reflecting the masking effect of the neighboring strong GSB and SE bands.

Small changes in the shape of the GSB feature were seen over time, particularly at around 620 nm. These changes could reflect a charge-separation process. The decay-associated TA spectra of **MgCl−P1** that resulted from a global fitting revealed the presence of two decay components with lifetimes of 5.8 and 182 ps, respectively (see the Supporting Information, Figure S4).[31] The first of their corresponding extracted spectra revealed a negative peak centered at 615 nm, which evolved with a lifetime of 5.8 ps, thereby leading to a loss of the negative amplitude at 615 nm and a concurrent gain in the amplitude of the negative bands at 570 and 660 nm and of the positive band at 470 nm. The slower decay component, with a lifetime of 182 ps, which was observed in the TA-decay profiles, was similar to the fluorescence lifetime of **MgCl−P1** ($\tau_{fl} = 258$ ps; Table 1 and the Supporting Information, Figure S9).

These spectroscopic changes lead us to suggest the formation of different excited states that are characterized by different lifetimes and, hence, decay timescales. The TA spectroscopic features of **MgCl−P2** and **MgCl−P4** are essentially the same and, thus, are independent of the substituents (at least in the case of these two complexes). The decay-time constants, as deduced from the global fit, also match well with the fluorescence lifetimes for **MgCl−P2** and **MgCl−P4** (Table 1 and the Supporting Information, Figure S9).

In the case of the non-emissive derivative, **MgCl−P3**, a very weak positive signal at 670 nm was observed after 10 ps in the TA spectra. This feature is ascribed to the formation of a charge-separated species, which arises from a photoinduced electron-transfer process analogous to what was inferred in the case of **H−P3** (see above). Unfortunately, owing to the ultrafast decay ($\tau_e = 26$ ps) associated with the proposed charge-transfer event, the decay-associated TA spectra of **MgCl−P3** could not be extracted by using a standard global analysis (see the Supporting Information, Figure S6).

Photoinduced electron transfer and Gibbs energy considerations: As inferred from the TA spectra of **H−P*n*** and their Mg adducts, photoinduced electron-transfer (PET) processes are expected to participate in the excited-state dynamics of all of these derivatives. This result is consistent with emissive behavior that is eventually governed by donor-excited PET (d-PET) processes,[32] owing to electron transfer from the excited fluorophore (i.e., the dipyrrin core) to the acceptor moiety (i.e., 1,10-phenanthroline).[33] Support for this suggestion comes from the work of Nagano, Fukuzumi, and co-workers, who reported the direct observation of radical-ion pairs of fluorescein-based probes by using EPR spectroscopy.[32a] Thus, the EPR spectrum of **MgCl−P1** was recorded with photoirradiation at 77 K. Under these conditions, a characteristic active signal was seen at $g = 2.003$. The observation of this signal is fully consistent with the proposed photoinduced formation of charge-separated radical species (Figure 5 and the Supporting Information, Figure S11).

Although the corresponding radical cation of the electron-donor moiety and the radical anion of the fluorophore could not be assigned owing to signal broadening, a remarkable substitution effect was observed in the intensities of the ESR signals of **MgCl−P*n***. The relatively more strongly fluo-

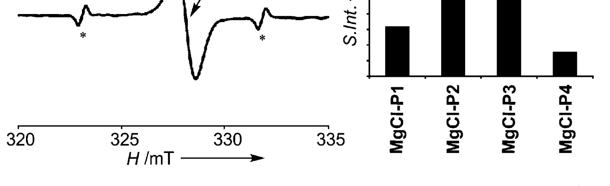

Figure 5. ESR spectrum measured of a) **MgCl−P1** at 77 K (1.0×10^{-3} M in a frozen solution of MeCN) under photoirradiation with a high-pressure Hg lamp. Asterisk (*) denotes a Mn^{2+} marker. b) Difference between the spin-signal intensities of the radicals in each **MgCl−P*n*** complex.

rescent derivative **MgCl−P4** gave rise to a weak signal in the spectrum, whereas the almost-non-fluorescent adduct **MgCl−P3** exhibited a strong signal under the same irradiation conditions. These effects of substitution on the intensities of the ESR signals leads us to suggest that the d-PET process from the dipyrrin unit (fluorophore) to the 1,10-phenanthroline (acceptor) is abetted by the electron-donating nature of **MgCl−P3**. In contrast, in **MgCl−P4**, the corresponding d-PET was inhibited, owing to the contrasting electronic inductive effects. On this basis, we conclude that the emission properties of these Mg adducts (**MgCl−P*n***) are strongly affected by the substituents at the *meso* and β-pyrrolic positions.

The inherent feasibility of electron transfer between an excited-state sensitizer and a quencher can be analyzed in terms of the change in free energy (ΔG_{eT}). The ΔG_{eT} values were calculated from the Rehm–Weller equation, as shown in Equation (1),[34] where E_{ox} and E_{red} are the oxidation and reduction potentials of the electron donor and acceptor, respectively, ΔE_{0-0} is the singlet-excited energy, and w_p is the electrostatic interaction energy in the radical ion pair, which corresponds to the work term for charge separation.

$$\Delta G_{eT} = E_{ox} - E_{red} - \Delta E_{0-0} - w_p \tag{1}$$

For contact radical ion pairs, the w_p value can be evaluated as $-e^2/\varepsilon r$, where ε is the dielectric constant of the solvent ($\varepsilon = 38$) and r is the distance between the electron donor and -acceptor.[32a] The r value was estimated to be about 5.5 Å from the crystal structure of **ZnCl−P1**. We assumed that the **MgCl−P*n*** complexes possessed the same value of w_p (0.07 eV) as the crystallographically characterized zinc complex.

To evaluate the corresponding energies of derivatives **H−P*n*** and **MgCl−P*n***, cyclic voltammetry (CV) and differential pulse voltammetry (DPV) analyses were carried out in MeCN that contained 0.1 M tetrabutylammonium hexafluorophosphate ($TBAPF_6$) as the electrolyte (Table 2). From the redox potentials and optical data, the relative ΔG_{eT} values of **MgCl−P*n*** were calculated to be −0.32 eV for **MgCl−P1**, −0.34 eV for **MgCl−P2**, −0.51 eV for **MgCl−P3**, and −0.33 eV for **MgCl−P4**, respectively. Thus, in all of these cases, the proposed electron-transfer process was exergonic in MeCN (Table 2) and was most favorable (in a thermodynamic sense) in the case of **MgCl−P3**. On this basis, the fluorescence-quenching of the **MgCl−P*n*** complexes and the **H−P*n*** ligands from which they derive is thought to most-probably arise from a rapid internal d-PET process. Based on the structure-dependent nature of the quenching, the specific d-PET events are thought to reflect variations in the peripheral substituents (Figure 6).

Table 2. Electrochemical data and parameters of the electron-transfer energies of **H−P*n*** and **MgCl−P*n***[a] (*V* versus SCE).

Compound	Oxidation		Reduction		ΔE[b]	E_{0-0}[c]	ΔG_{ET}[d]
	$E^{ox}(1)$	$E^{ox}(2)$	$E^{red}(1)$	$E^{red}(2)$			
H−P1	1.09	1.42	−0.78	−1.09	1.87	2.32	−0.52
H−P2	1.08	1.40	−0.81	−1.09	1.89	2.32	−0.50
H−P3	0.86	1.31	−0.97	−1.34	1.83	2.26	−0.50
H−P4	1.21	1.46	−0.70	−0.99	1.91	2.30	−0.46
MgCl−P1	1.00	1.42	−0.81	−1.07	1.81	2.06	−0.32
MgCl−P2	0.97	1.42	−0.81	−1.09	1.78	2.05	−0.34
MgCl−P3	0.81	1.29	−0.95	−1.29	1.76	2.20	−0.51
MgCl−P4	1.06	1.46	−0.73	−1.06	1.79	2.05	−0.33

[a] These values were determined by DPV by using a platinum working electrode, a platinum wire counter electrode, and a Ag/Ag^+ reference electrode in MeCN solution that contained 0.1 M $TBAPF_6$ as a supporting electrolyte. Scan rate: 0.1 $V s^{-1}$. [b] Energy gap [$E^{ox}(1)-E^{red}(1)$]. [c] Zero–zero excitation energy. [d] Change in free energy, as calculated by using the Rehm–Weller equation.

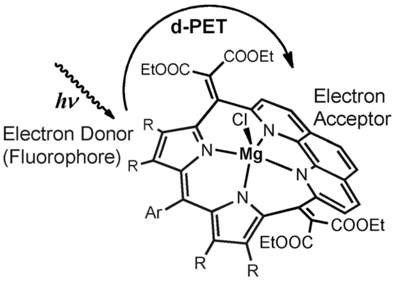

Figure 6. Schematic representation of d-PET from the dipyrrin- to 1,10-phenanthroline fragments in **MgCl−P*n***. The directly linked *meso*-aryl(Ar) and β-(R) substituents on the dipyrrin unit can control the d-PET effect.

Charge-transfer properties as characterized by DFT calculations: To understand better the relevant photophysical properties and the presumed d-PET events seen upon photoexcitation of **H−P*n*** and **MgCl−P*n***, their frontier molecular orbitals (MO) were generated at the B3LYP/6-31G(d) level (Figure 7 and the Supported Information, Figures S12 and S13). Likewise, their corresponding electronically excited states were calculated by using time-dependent DFT analyses carried out at the B3LYP/6–31+G(d) level (see the Supporting Information, Table S2 and Figure S14). As reported previously,[4] both the HOMO and LUMO of **H−P1** are exclusively centered on the dipyrrin subunit with sizable contributions from the exocyclic double-bond moieties. Based on the associated TD-DFT calculations, the lowest-energy HOMO–LUMO transition in **H−P1** corresponds to a π–π* excited state, in analogy to what is true for the BODIPYs.[9]

The electron distribution in the LUMO of **MgCl−P*n*** shows a significant penetration of the electron density into the 1,10-phenathroline unit. This overlap is considered to be directly reflective of the proposed charge-transfer character. Moreover, the electron density in the LUMO+1 of these magnesium complexes is almost exclusively centered on the 1,10-phenanthroline moiety. On this basis, we propose that the experimentally observed fluorescence quenching in the case of **MgCl−P2** and **MgCl−P3** reflects partial charge transfer from the Mg–dipyrrin subunit to the 1,10-phenanthroline moiety upon photoexcitation.

To quantify the change in electron distribution over the dipyrrin and 1,10-phenanthroline moieties in **MgCl−P*n***,

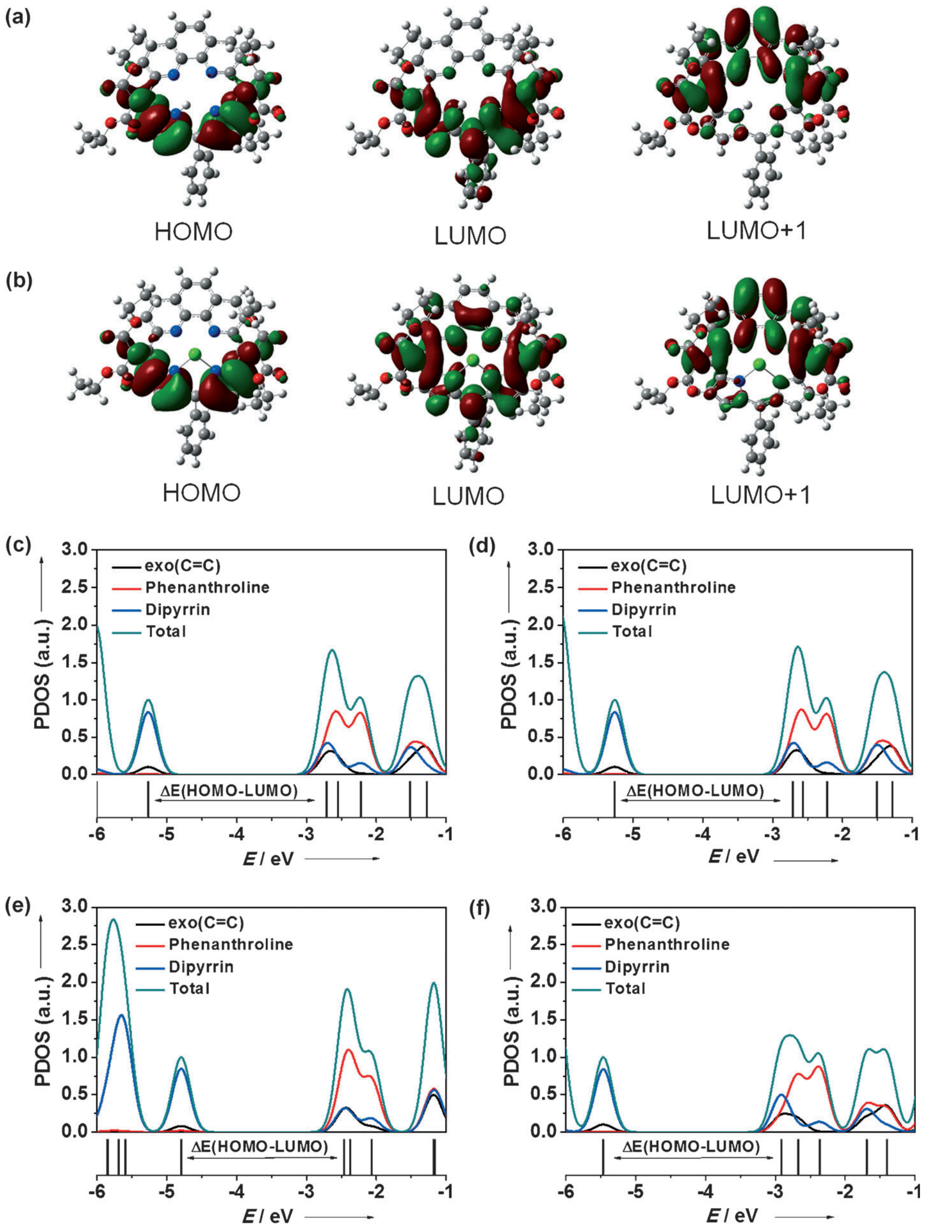

Figure 7. Representations of the HOMO, LUMO, and LUMO+1 of a) **H−P1** and b) **MgCl−P1**. Partial density-of-state (PDOS) diagrams for c) **MgCl−P1**, d) **MgCl−P2**, e) **MgCl−P3**, and f) **MgCl−P4**, in which the *exo*-cyclic carbon−carbon (exo C=C, black), dipyrromethene (dipyrrin, blue) and 1,10-phenanthroline moieties (phenanthroline, red) are considered as individual groups (Scheme 1).

Mulliken population analysis was carried out by using the GaussSum program.[35] Density-of-states (DOS) spectra provide a pictorial representation of the MO contributions to the overall electron densities. The DOS diagrams (Figure 7) and the content of electron distribution (see the Supporting Information, Table S2) lead us to suggest that the HOMOs mainly reflect dipyrrin-based density (84–88 %) with a minor component from the *exo*-cyclic C=C bonds (6–10 %). In contrast, the LUMOs are mixed and have contributions from the 1,10-phenanthroline-, *exo*-C=C-, and dipyrrin groups. Importantly, the electron distributions on the 1,10-phenanthroline and dipyrrin portions in the LUMOs depend on the nature of the *meso*- and *β*-substituents: the contribution of the 1,10-phenanthroline moiety in **MgCl−P1** (24 %), **MgCl−P2** (25 %), **MgCl−P3** (39 %), and **MgCl−P4** (17 %) is substantial, whereas those of the dipyrrin are estimated to be 39 %, 39 %, 27 %, and 49 %, respectively. These results lead us to suggest that increased electron density within the dipyrrin portion of the LUMO, as seen in the case of electron-deficient derivative **MgCl−P4**, favors an emissive π–π* transition because of the stronger MO overlap with the dipyrrin fluorophore (i.e., HOMO–LUMO transition; cf. the Supporting Information, Table S2). In other words, the $S_0 \rightarrow S_1$ transition, which involves a partially "dark" charge transfer from the dipyrrin (donor) to 1,10-phenanthroline (acceptor) fragment, is dominated by the electronic structure of the dipyrrin subunit.[36]

In accord with the above expectations, the transitions from the HOMO to the LUMO−1 in these magnesium complexes are thought to reflect an effective electron-transfer process (that involves charge transfer from the dipyrrin donor to the 1,10-phenanthroline acceptor). Thus, the oscillator strengths (*f*) of **MgCl−P*n*** become larger as the electron-donating ability of the dipyrrin unit increases (see the Supporting Information, Table S2 and Figure S14). The direction of the dipole moment in **MgCl−P*n***, namely from the dipyrrin to the 1,10-phenanthroline moiety (see the Supporting Information, Figure S15), is consistent with the proposed d-PET.[37] From a purely structural perspective, the smaller dihedral angle about the *meso*-exocyclic double bonds between the dipyrrin and 1,10-phenathroline units may enhance the super-exchange interactions between these key subunits upon Mg^{2+} complexation.[27b] The increased structural rigidity that is provided by Mg^{2+} complexation could also contribute to the spectroscopic effects that are ascribable to d-PET. In fact, the increase in emission at low temperatures and the attendant increase in structural rigidity are consistent with a "turning off" of nonradiative decay pathways and an attendant enhancement of emissive transitions.[38]

Conclusions

In this study, we have described the synthesis and characterization of 1,10-phenanthroline-embedded porphyrin analogues, **H−P*n***, that bear substituents at the peripheral *meso* and β-positions of the embedded dipyrrin moieties. As inferred from the crystal structure of zinc-chloride complex **ZnCl−P1** and from fluorescence spectroscopy of magnesium complexes **MgX−P1**, which contain different axial counteranions (e.g. $X = ClO_4$, OAc, Cl, Br, I), the Mg-adducts adopt a square-pyramidal geometry about the metal center, in which the fifth ligation site is occupied by an axially coordinated counteranion. The introduction of peripheral substituents at the *meso* and β-pyrrole positions of the parent system allowed for the preparation of three new analogues, **H−P*n*** ($n = 2$–4). These modifications gave rise to discernible differences between their physicochemical properties, including cation-binding affinities, emission efficiencies, excited-state dynamics, and redox potentials. Detailed EPR and TA spectroscopic studies of the photoinduced charge-separated species in **MgCl−P*n*** provided support for the notion that the emissive properties of **MgCl−P*n*** are partially governed by an internal d-PET process from the dipyrrin subunit to the 1,10-phenanthroline moiety. This conclusion was supported by theoretical calculations, which revealed charge transfer in the context of the principle HOMO–LUMO transitions. Currently, d-PET-based fluorescent sensors are still rare[39] and their application to the problem of Mg^{2+}-ion sensing is, to the best of our knowledge, without precedent. Thus, this study is expected to contribute to our fundamental understanding of the electronic features of hybrid macrocyclic porphyrin systems, in particular, the design principles that control internal-charge-transfer processes, whilst setting the stage for the synthesis of improved Mg^{2+}-sensor systems.

Experimental Section

Instruments: ^{1}H NMR spectra were recorded on a JEOL JMX-GX400 (400 MHz) spectrometer. ^{13}C NMR and ^{19}F NMR spectra were recorded on a JEOL ECA500 (500 MHz) spectrometer. Chemical shifts (δ) are reported with reference to residual non-deuterated chloroform ($\delta = 7.26$ ppm for the ^{1}H NMR spectra, $\delta = 65.00$ ppm for the ^{13}C NMR spectra) and $CFCl_3$ ($\delta = 0.00$ ppm for the ^{19}F NMR spectra). High-resolution mass spectra (HRMS) were recorded on a JEOL LMS-HX-110 spectrometer. MS (FAB) spectra were measured by using 3-nitrobenzyl alcohol (NBA) as the matrix. UV/Vis absorption spectra were recorded on a Shimadzu UV-3100PC spectrometer. Fluorescence spectra were recorded on a Shimadzu RF-5300PC spectrophotometer. Temperature-dependent fluorescent spectra were determined by using a UNISOKU cryostat temperature controller.

Materials: Unless otherwise noted, chemicals and reagents were purchased from commercial suppliers and used without further purification. Certain precursors, including pyrrole, mesitylaldehyde, and benzaldehyde, were purified by distillation in vacuo. All solvents were used after appropriate distillation or purification. All metal salts for titration experiments were of the highest available purity. Analytical thin-layer chromatography (TLC) was performed on Merck silica gel 60 pre-coated aluminum sheets. Column chromatography was either carried out on silica gel 60N (60 mesh, KANTO chemical) or on neutral alumina (Wako chemical). 6,18-Bis(diethoxycarbonylmethylidene)-1-phenyl-phenanporphodimethene (**H−P1**)[4] and *meso*-aryldipyrromethanes (**2b**,**c**)[40] were prepared according to literature procedures.

Synthesis of 6,18-bis(diethoxycarbonylmethylidene)-1-mesityl-phenanporphodimethene (H−P2): Compound **H−P2** was prepared by using a [2+2]-type condensation similar to that used to prepare **H−P1**.[4] Compound **1** (0.5 g, 9.77×10^{-4} mol) and 5-mesityl-dipyrromethane (**2b**, 256 mg, 9.77×10^{-4} mol) were dissolved in CH_3CN (200 mL) and then trifluoroacetic acid (TFA, 1 mL) was added. The mixture was stirred for 3 days at room temperature. Then, 2,3-dichloro-5,6-dicyano-*p*-benzoquinone (DDQ, 0.665 g, 2.93×10^{-3} mol) and triethylamine (TEA, 2 mL) were added. The mixture was stirred for an additional 1 h and the solvent was removed in vacuo. The residue was passed through an alumina column ($CHCl_3$) and the first eluted red fraction was collected. Purification by column chromatography on silica gel ($MeOH/CHCl_3$, 2%) gave **H−P2** as a red powder. Yield: 480 mg (64%); ^{1}H NMR (400 MHz, $CDCl_3$): $\delta = 13.60$ (s, 1H; NH), 8.22 (d, $J = 8.3$ Hz, 2H; Phen-H), 7.85 (d, $J = 8.3$ Hz, 2H; Phen-H), 7.82 (s, 2H; Phen-H), 6.87 (s, 2H; Ar-H), 6.57 (d, $J = 4.3$ Hz, 2H; Pyrr-H), 6.26 (d, $J = 4.3$ Hz, 2H; Pyrr-H), 4.18 (dd, $J = 14.1$, 7.1 Hz, 4H; CH_2), 4.12 (dd, $J = 14.1$, 7.1 Hz, 4H; CH_2), 2.32 (s, 3H; Ar-CH_3), 1.98 (s, 6H; Ar-CH_3), 1.15 (t, $J = 7.1$ Hz, 6H; CH_3), 1.08 ppm (t, $J = 7.0$ Hz, 6H; CH_3); ^{13}C NMR (125 MHz, $CDCl_3$): $\delta = 166.04$, 163.69, 154.19, 145.57, 143.97, 142.70, 141.51, 137.64, 136.67, 135.08, 133.81, 128.85, 128.92, 127.86, 127.61, 127.42, 126.26, 120.47, 62.08, 61.77, 21.20, 20.02, 13.91, 13.84 ppm; HRMS (FAB): *m/z* calcd for $C_{46}H_{42}N_4O_8$: 778.3003; found: 778.2978; elemental analysis calcd (%) for $C_{46}H_{42}N_4O_8$: C 70.06, H 5.74, N 6.79; found: C 70.94, H 5.44, N 7.19.

Synthesis of 6,18-bis(diethoxycarbonylmethylidene)-1-phenyl-3,4,20,21-tetramethylphenanporphodimethene (H−P3): Compound **1** (0.5 g, 9.77×10^{-4} mol) and 5-phenyl-2,3,6,7-tetramethyldipyrromethane (**3c**, 267 mg, 9.77×10^{-4} mol) were treated under similar conditions to those mentioned above. The product was passed through an alumina column ($CHCl_3$), followed by column chromatography on silica gel ($MeOH/CHCl_3$, 3%) to give **H−P3** as a red powder. Yield: 395 mg (52%); ^{1}H NMR (400 MHz, $CDCl_3$): $\delta = 13.09$ (s, 1H; NH), 8.17 (s, 2H; Phen-H), 7.85 (d, $J = 8.3$ Hz, 2H; Phen-H), 7.73 (d, $J = 8.3$ Hz, 2H; Phen-H), 7.03–7.38 (m, 5H; Ph-H), 4.21 (br s, 4H; CH_2), 4.10 (br s, 4H; CH_2), 1.92 (s, 6H; β-CH_3), 1.19 (t, $J = 7.1$ Hz, 6H; CH_3), 1.10 (s, 6H; β-CH_3), 1.05 ppm (t, $J = 7.0$ Hz, 6H; CH_3); ^{13}C NMR (125 MHz, $CDCl_3$): $\delta = 165.18$, 164.08, 153.79, 148.75, 145.56, 144.62, 140.43, 139.92, 139.10, 135.51, 129.18, 128.81, 128.62, 128.42, 127.06, 125.93, 122.68, 62.12, 13.93, 13.90, 12.66, 11.08 ppm; HRMS (FAB): *m/z* calcd for $C_{47}H_{45}N_4O_8$: 793.3233; found: 779.3237; elemental analysis calcd (%) for $C_{47}H_{45}N_4O_8$: C 71.20, H 5.59, N 7.07; found: C 70.35, H 5.75, N 6.46.

Synthesis of 6,18-bis(diethoxycarbonylmethylidene)-1-pentafluorophenyl-phenanporphodimethene (H−P4): Compound **1** (0.5 g, 9.77×10^{-4} mol) and 5-pentafluorophenyldipyrromethane (**3d**, 300 mg, 9.77×10^{-4} mol) were treated under similar conditions to those mentioned above. This acid-induced cyclization reaction was allowed to continue for 5 days. Then, DDQ and TEA were added. Compound **H−P4** was obtained by using a purification procedure that was similar to that described above. Yield: 178 mg (22%); ^{1}H NMR (400 MHz, $CDCl_3$): $\delta = 13.59$ (s, 1H; NH), 8.10 (d, $J = 8.3$ Hz, 2H; Phen-H), 7.80 (d, $J = 8.3$ Hz, 2H; Phen-H), 7.79 (s, 2H; Phen-H), 6.70 (d, $J = 4.4$ Hz, 2H; Pyrr-H), 6.40 (d, $J = 4.4$ Hz, 2H; Pyrr-H), 4.21 (dd, $J = 14.1$, 7.1 Hz, 4H; CH_2), 4.11 (dd, $J = 14.1$, 7.1 Hz, 4H; CH_2), 1.19 (t, $J = 7.1$ Hz, 6H; CH_3), 1.06 ppm (t, $J = 7.0$ Hz, 6H; CH_3); ^{19}F NMR (470 MHz, $CDCl_3$): $\delta = -139.98$ (s, 2F), −151.93 (t, $J = 20.1$ Hz, 2F), −160.6 ppm (d, $J = 59.6$ Hz, 1F); ^{13}C NMR (125 MHz, $CDCl_3$): $\delta = 165.44$, 163.66, 153.85, 145.48, 143.23, 135.49, 135.46, 135.42, 129.81, 129.75, 127.66, 127.63, 126.52, 126.49, 124.19, 124.16, 62.33, 61.95, 13.89, 13.81 ppm; HRMS (FAB): *m/z* calcd for $C_{43}H_{31}F_5N_4O_8$: 826.2054; found: 826.2062; elemental analysis calcd (%) for $C_{46}H_{42}N_4O_8$: C 62.47, H 3.78, N 6.78; found: C 61.92, H 3.69, N 6.49.

Synthesis of zinc [6,18-Bis(diethoxycarbonylmethylidene)-1-phenyl-phenanporphodimethene] chloride (ZnCl−P1): Compoiund **H−P1** (100 mg, 1.26×10^{-4} mol) was dissolved in $CHCl_3$ (50 mL) and a solution that contained an excess of $ZnCl_2$ and a few drops of 2,6-lutidine in MeOH (10 mL) was added. After the mixture had been heated for 10 min with stirring, the color of the solution became dark purple. The mixture was concentrated by using a rotary evaporator and then the residue was extracted with $CHCl_3$ and washed with water, an aqueous solution of Na_2CO_3, and brine. The organic layer was dried with Na_2SO_4 and the solvent was removed under reduced pressure. The resulting products were purified by column chromatography on silica gel (CH_2Cl_2/MeOH, 100:3). The second set of purple fractions were collected and concentrated to afford the pure product, **ZnCl−P1**. Yield: 57.8 mg (55 %); ^{1}H NMR (500 MHz, CD_2Cl_2): $\delta=8.06$ (d, $J=8.3$ Hz, 2H; Phen-H), 7.96 (d, $J=8.3$ Hz, 2H; Phen-H), 7.60–7.62 (m, 1H; Phenyl-H), 7.47 (dt, $J=4.0$, 0.9 Hz, 2H; Phenyl-H), 7.38 (s, 2H; Phen-H), 7.34–7.37 (m, 1H; Phenyl-H), 7.26 (dd, $J=7.7$, 0.9 Hz, 1H; Phenyl-H), 6.80 (d, $J=4.0$ Hz, 2H; Pyrr-H), 6.66 (d, $J=4.0$ Hz, 2H; Pyrr-H), 4.20–4.37 (m, 8H; CH_2), 1,29 (t, $J=7.2$ Hz, 6H; CH_3), 1.22 ppm (t, $J=7.2$ Hz, 6H; CH_3); ^{13}C NMR (125 MHz, CD_2Cl_2): $\delta=164.86$, 163.11, 153.54, 152.97, 149.64, 143.37, 140.94, 140.02, 138.23, 137.68, 132.77, 131.32, 130.87, 130.58, 127.48, 127.28, 126.80, 126.34, 119.82, 62.52, 62.43, 13.80, 13.72 ppm; HRMS (FAB): m/z calcd for $C_{43}H_{35}N_4O_8Zn_1$: 799.1746 [M−Cl]; found: 799.1744; UV/Vis (CH_2Cl_2): λ_{max} ($\log\varepsilon$) = 571 nm (4.54); elemental analysis calcd (%) for $C_{43}H_{35}N_4O_8Zn_1$: C 61.73, H 4.22, N 6.70; found: C 60.58, H 4.40, N 6.41.

Spectroscopic measurements: Stock solutions of **H−P*n*** were prepared in dry MeCN (2.0×10^{-5} M unless otherwise noted). Solutions of the cation salts were prepared in absolute MeOH with a fixed concentration and then diluted with dry MeCN. For the spectroscopic studies, about 2 mL of the stock solution of **H−P*n*** was placed in a quartz cell with a 1 cm optical-path length. Increasing known quantities of the stock solution that contained the cation of interest were then added dropwise into the quartz cell by using a microsyringe. The fluorescent quantum yields were determined by comparison to tetraphenylporphyrin ($\Phi_{fl}=0.065$), which was taken as a standard.[41]

Electrochemical measurements: Cyclic voltammetric measurements were carried out on a CHI 620D electrochemical analyzer with a conventional three-electrode cell. A solution of the sample (about 1 mM) in dry MeCN that contained 0.1 M nBu$_4$NPF$_6$ (TBAPF$_6$) was then loaded into the cell and an argon atmosphere was established. A Pt disc working electrode, a Pt wire counter electrode, and a Ag/AgNO$_3$ reference electrode were used. The potentials were calibrated by using ferrocene but are reported relative to the SCE by adding 0.29 V to the “raw” measured values. The spectroelectrochemical experiments reported herein were performed in a thin-layer spectroelectrochemical quartz cell (path length: 2 mm) by a using a three-electrode arrangement, that is, a light-transparent Pt gauze as a working electrode, a Pt wire counter electrode, and a Ag/AgNO$_3$ reference electrode. The changes in absorption features during the associated experiments were monitored on a Varian Cary-5000 UV/Vis/NIR spectrometer.

Determination of the binding constants for Mg^{2+} ion: To determine the binding constant (K_{Mg}), the fluorescence intensity was recorded as a function of cation concentration (see the Supporting Information, Figure S3). The changes were analyzed by using a nonlinear curve-fitting that was based on 1:1 binding stoichiometry, according to Equation (2),[42] where A and A_0 are the absorption intensities of ligand **H−P*n*** in the presence- and absence of metal cations (M^{2+}), C_M and C$_L$ are the concentrations of M^{2+} and **H−P*n***, and K_S is the binding constant.

$$A/A_0 = 1+(A_{max}/2A_0-1/2)\{1+C_M/C_L+1/K_SC_L -[(1+C_M/C_L+1/K_SC_L)^2-4C_M/C_L]^{1/2}\} \qquad (2)$$

Femtosecond transient-absorption measurements: The femtosecond time-resolved transient-absorption (TA) spectrometer consisted of a homemade noncollinear optical parametric amplifier (NOPA) that was pumped by a Ti:sapphire regenerative amplifier system (Quantronix, Integra-C), which operated at a 1 kHz repetition rate, and an accompanying optical-detection system. The generated visible NOPA pulses, which were used as the pump pulses, had a pulse width of about 100 fs and an average power of 1 mW in the range 450–800 nm. White-light-continuum (WLC) probe pulses were generated by using a sapphire window (2 mm thick) by focusing a small portion of the fundamental 800 nm pulses, which were picked off by a quartz plate before entering into the NOPA. The time delay between the pump and the probe beams was carefully controlled by making the pump beam travel along a variable optical delay (Newport, ILS250). Intensities of the spectroscopically dispersed WLC probe pulses were monitored on a miniature spectrograph (OceanOptics, USB2000+). To obtain the time-resolved transient absorption difference signal (ΔA) at a specific time, the pump pulses were chopped at 25 Hz and the intensities of the absorption spectra were alternately saved, either with or without subjection to the pump pulse. Typically, 6000 pulses were used to excite the samples and to obtain the TA spectra at a particular delay time. The polarization angle between the pump and the probe beams was set at the magic angle (54.7°) by using a Glan-laser polarizer with a half-wave retarder to prevent polarization-dependent signals. The cross-correlation fwhm in the pump-probe experiments was less than 200 fs and the chirp of WLC probe pulses was 800 fs in the 400–800 nm region. To minimize chirp, all-reflection optics were used in the probe beam-path and a quartz cell with a path length of 2 mm was employed. After completing each set of fluorescence and TA experiments, the absorption spectra of all of the compounds were carefully checked to rule out the presence of artifacts or spurious signals that may arise from, for example, degradation or photo-oxidation of the samples in question.

ESR detection of the photoexcited species: ESR spectroscopy of the photoexcited Mg adducts was carried out on a JEOL JES-TE 300 spectrometer. To detect the transient radical species in frozen solutions of **MgCl−P*n*** in MeCN at 77 K, frozen glass solutions were made up in quartz EPR tubes and subjected to photoirradiation with a high-pressure mercury lamp (USHIO SX-U1501HR). The magnetic field was calibrated from the hyperfine coupling constants of the Mn^{II} ion that was present as a dopant in a MgO powder matrix (86.9 Gauss).

X-ray crystallography: Single crystals of **ZnCl−P1** were grown from a CH_2Cl_2/MeOH mixture. X-ray diffraction analysis was carried out on a Rigaku RAXIS RAPID instrument that was equipped with an imaging plate area detector by using graphite-monochromated Mo$_{K\alpha}$ radiation ($\lambda=0.71075$ Å). For **ZnCl−P1** ($2\theta=54.8°$), the data were collected at −140 °C. Corrections were made for both Lorentzian and polarization effects. The structures were solved by using direct methods (SIR 97 program) and were refined anisotropically for non-hydrogen atoms through use of full-matrix least-squares calculations. All hydrogen atoms were located at their calculated positions and they were assigned a fixed displacement and constrained to ideal geometry with C−H = 0.95 Å. The crystallographic calculations were performed by using the Crystal Structure software package of the Rigaku Corporation.[43]

Nanosecond time-resolved fluorescence-decay measurements: Time-resolved fluorescence-lifetime experiments were performed by using time-correlated single-photon-counting (TCSPC). As an excitation light source, we used a homemade cavity-dumped Ti:sapphire oscillator, which provided a high repetition rate (200–400 kHz) of ultrashort pulses (100 fs at full-width at half-maximum (fwhm)) that were pumped by a continuous-wave (cw) Nd-YVO4 laser (Coherent, Verdi). The output pulse of the oscillator was frequency-doubled by a second harmonic crystal (thickness: 1 mm, barium borate, BBO, CASIX). The fluorescence was collected by a microchannel-plate photomultiplier (MCP-PMT, Hamamatsu, R3809U-51) with a thermoelectric cooler (Hamamatsu, C4878) that was connected to a TCSPC board (Becker&Hickel SPC-130). The overall instrumental response function was about 25 ps (fwhm). A vertically polarized pump pulse by a Glan-laser polarizer irradiated the samples and a sheet polarizer that was set at an angle that was complementary to the magic angle (54.7°) was placed in the fluorescence-collection pathway to obtain polarization-independent fluorescence decays.

DFT calculations: All calculations were carried out with the Gaussian 03 software package.[44] Energy calculations and geometry optimizations for all of the molecules that were considered in this study, that is, **H−P*n*** and **MgCl−P*n***, were performed by using the B3LYP DFT method with the 6–

31G (d) basis set without any symmetry restrictions.[45] Then, the optimized geometries were used as the starting point for time-dependent (TD-DFT) calculations of the excited-state energies and oscillator strengths by using the 6–31+G (d) basis set and electron-population analysis with the 6–31G (d) basis set. All molecular orbitals were visualized with the software GaussView 5.0. The GaussSun 2.2 software package[35] was used to calculate group contributions to the molecular orbitals to prepare the partial density-of-states (PDOS) spectra. The contribution of a group to a molecular orbital was calculated within the framework of Mulliken population analysis. The PDOS spectra (see the Supporting Information) were created by convoluting the molecular-orbital information with Gaussian curves of unit height and fwhm = 0.3 eV.

Acknowledgements

This work at Kyushu University was financially supported by the Global COE Program, "Science for Future Molecular Systems", funded by the MEXT (Ministry of Education, Culture, Sports, Science and Technology) of Japan and by a Grant-in-Aid for Scientific Research (S) (no. 17105003 to Y.N.), funded by the Japan Society for the Promotion of Science (JSPS). The research at Yonsei University was supported by the Mid-Career Researcher (2010–0029668) and WCU (World Class University) programs (R32–2010–000–10217–0), which were administered through the National Research Foundation of Korea and funded by the Ministry of Education, Science and Technology (MEST), as well as by an AFSOR/AOARD grant (no. FA2386–09–1–4092 to D.K.). Support from the National Science Foundation (grant no. CHE 105790 to J.L.S.) and the Robert A. Welch Foundation (grant F-1018 to J.L.S.) is also gratefully acknowledged. The authors thank Prof. Teruo Shinmyozu (Kyushu University, Japan) for allowing us access to his photoirradiation apparatus and acknowledge Prof. Chang-Hee Lee (Kangwon National University, Korea) for his valuable advice and comments on this work. The computational studies were carried out by using the computer facilities at the Research Institute for Information Technology, Kyushu University, which is a shared resource that we would like to acknowledge here.

---

[1] a) V. Trapani, G. Farruggia, C. Marraccini, S. Iotti, A. Cittadini, F. I. Wolf, *Analyst* **2010**, *135*, 1855; b) Y. Shindo, T. Fujii, H. Komatsu, D. Citterio, K. Hotta, K. Suzuki, K. Oka, *PloS ONE* **2011**, *6*, e23684, and references therein.

[2] a) E. Andrasi, N. Pali, Z. Molnar, S. Kosel, *J. Alzheimer's Dis.* **2005**, *7*, 273; b) M. D. Boska, *Neurology* **2002**, *58*, 1227; c) M. Yasui, T. Kihira, K. Oka, *Neurotoxicology* **1992**, *13*, 593.

[3] For charged β-diketones, see: a) Y. Suzuki, H. Komatsu, T. Ikeda, N. Saito, S. Araki, D. Citterio, H. Hisamoto, Y. Kitamura, T. Kubota, J. Nakagawa, K. Oka, K. Suzuki, *Anal. Chem.* **2002**, *74*, 1423; b) T. Shoda, K. Kikuchi, H. Kojima, Y. Urano, H. Komatsu, K. Suzuki, T. Nagano, *Analyst* **2003**, *128*, 719; c) H. Komatsu, N. Iwasawa, D. Citterio, Y. Suzuki, T. Kubota, K. Tokuno, Y. Kitamura, K. Oka, K. Suzuki, *J. Am. Chem. Soc.* **2004**, *126*, 16353; d) H. M. Kim, P. R. Yang, M. S. Seo, J. S. Yi, J. H. Hong, S. J. Jeon, Y. G. Ko, K. J. Lee, B. R. Cho, *J. Org. Chem.* **2007**, *72*, 2088; for diaza[18]crown-6, see: e) G. Farruggia, S. Iotti, L. Prodi, M. Montalti, N. Zaccheroni, P. B. Savage, V. Trapani, P. Sale, F. I. Wolf, *J. Am. Chem. Soc.* **2006**, *128*, 344; benzo[15]crown-5: f) H. Hama, T. Morozumi, H. Nakamura, *Tetrahedron Lett.* **2007**, *48*, 1859; for calix[4]arene, see: g) K. C. Song, M. G. Choi, D. H. Ryu, K. N. Kim, S. K. Chang, *Tetrahedron Lett.* **2007**, *48*, 5397; for imine-containing aromatic compounds, see: h) D. Ray, P. K. Bharadwaj, *Inorg. Chem.* **2008**, *47*, 2252; i) N. Singh, N. Kaur, R. C. Mulrooney, J. F. Callan, *Tetrahedron Lett.* **2008**, *49*, 6690; j) Y. Dong, X. Mao, X. Jiang, J. Hou, Y. Cheng, C. Zhu, *Chem. Commun.* **2011**, *47*, 9450; k) Y. Dong, J. Li, X. Jiang, F. Song, Y. Cheng, C. Zhu, *Org. Lett.* **2011**, *13*, 2252; l) Z. Liu, H. Xu, C. Song, D. Huang, L. Sheng, R. Shi, *Chem. Lett.* **2011**, *40*, 75; m) X. Zhu, C. He, D. Dong, Y. Liu, C. Duan, *Dalton Trans.* **2010**, *39*, 10051.

[4] M. Ishida, Y. Naruta, F. Tani, *Angew. Chem.* **2010**, *122*, 95; *Angew. Chem. Int. Ed.* **2010**, *49*, 91.

[5] a) A. Loudet, K. Burgess, *Chem. Rev.* **2007**, *107*, 4891; b) G. Ulrich, R. Ziessel, A. Harriman, *Angew. Chem.* **2008**, *120*, 1202; *Angew. Chem. Int. Ed.* **2008**, *47*, 1184, and references therein.

[6] T. E. Wood, A. Thompson, *Chem. Rev.* **2007**, *107*, 1831.

[7] a) I. V. Sazanovich, C. Kirmaier, E. Hindin, L. Yu, D. F. Bocian, J. S. Lindsey, D. Holten, *J. Am. Chem. Soc.* **2004**, *126*, 2664; b) Y. Ding, Y. Xie, X. Li, J. P. Hill, W. Zhang, W. Zhu, *Chem. Commun.* **2011**, *47*, 5431; c) M. A. Filatov, A. Y. Lebedev, S. N. Mukhin, S. A. Vinogradov, A. V. Cheprakov, *J. Am. Chem. Soc.* **2010**, *132*, 9552; d) J. M. Sutton, E. Rogerson, C. J. Wilson, A. E. Sparke, S. J. Archibald, R. W. Boyle, *Chem. Commun.* **2004**, 1328; e) Y. Mei, C. J. Frederickson, L. J. Giblin, J. H. Weiss, Y. Medvedeva, P. A. Bentley, *Chem. Commun.* **2011**, *47*, 7107; see also ref. [23].

[8] C. Ikeda, S. Ueda, T. Nabeshima, *Chem. Commun.* **2009**, 2544.

[9] V. S. Thoi, J. R. Stork, D. Magde, S. M. Cohen, *Inorg. Chem.* **2006**, *45*, 10688.

[10] J. Kobayashi, T. Kushida, T. Kawashima, *J. Am. Chem. Soc.* **2009**, *131*, 10836.

[11] N. Sakamoto, C. Ikeda, M. Yamamura, T. Nabeshima, *J. Am. Chem. Soc.* **2011**, *133*, 4726.

[12] C. Bronner, S. A. Baudron, M. W. Hosseini, C. A. Strassert, A. Guenet, L. D. Cola, *Dalton Trans.* **2010**, *39*, 180.

[13] J. D. Hall, T. M. McLean, S. J. Smalley, M. R. Waterland, S. G. Telfer, *Dalton Trans.* **2010**, *39*, 437.

[14] K. Hanson, A. Tamayo, V. V. Diev, M. T. Whited, P. I. Djurovich, M. E. Thompson, *Inorg. Chem.* **2010**, *49*, 6077.

[15] When Mg^{2+} salts were added to a solution of the simple dipyrrin, no spectroscopic response was observed. This result is consistent with the literature; see reference [7f]. Furthermore, Bucher's stability index also predicts a low stability for the Mg–porphyrin complex; see: J. W. Buchler in *Porphyrins and Metalloporphyrins* (Ed.: K. M. Smith), Elsevier, Dordrecht, **1979**, pp. 197.

[16] Y. Shen, U. Ryde, *Chem. Eur. J.* **2005**, *11*, 1549.

[17] M. J. Bain-Ackerman, D. K. Lavallee, *Inorg. Chem.* **1979**, *18*, 3358.

[18] R. D. Shannon, *Acta Crystallogr. Sect. A.* **1976**, *32*, 751.

[19] J. Tammiku, P. Burk, A. Tuulmets, *J. Phys. Chem. A* **2001**, *105*, 8554.

[20] M. Ishida, Y. Naruta, F. Tani, *Dalton Trans.* **2010**, *39*, 2651.

[21] Such a counterion-dependence on the formation of the metal complex is probably due to the difference in the coordination modes of the magnesium-acetate salt. The oxygen atoms of the acetate anion coordinate to the metal center in a bidentate fashion; the acetate anion might complex to the metal center more effectively than other monodentate cations. See: a) L. Walter-Levy, I. Soleilhavoup, P. Maarten de Wolff, *C. R. Acad. Sci.* **1959**, *249*, 1234; b) G. B. Guseva, E. V. Antina, A. I. V'yugin, G. M. Mamardashvili, V. V. Petrov, *Russ. J. Coord. Chem.* **2006**, *32*, 116.

[22] a) C. Bucher, D. Seidel, V. Lynch, V. Král, J. L. Sessler, *Org. Lett.* **2000**, *2*, 3103; b) R. Myśliborski, L. Latos-Grażyński, L. Szterenberg, *Eur. J. Org. Chem.* **2006**, *14*, 3064.

[23] Crystallographic data for **ZnCl−P1**: $C_{44}H_{36}O_8N_4ZnCl_4$; crystal dimensions: $0.56\times0.25\times0.08\ mm^3$; monoclinic; space group $P2_1/a$; $a = 12.487(3)$, $b = 16.609(4)$, $c = 20.504(5)$ Å; $\beta = 95.018(19)^\circ$; $V = 4236(17)$ Å^3; $Z = 4$; $\rho_{calcd} = 1.499\ g\,cm^{-3}$; $F(000) = 1960$; $R_1 = 0.043$ ($I > 2.0\sigma(I)$); $R_w = 0.105$ (all data); GOF = 1.068. CCDC-881769 (**ZnCl−P1**) contains the supplementary crystallographic data for this paper. These data can be obtained free of charge from The Cambridge Crystallographic Data Centre via www.ccdc.cam.ac.uk/data_request/cif.

[24] H. Maeda, M. Hasegawa, T. Hashimoto, T. Kakimoto, S. Nishio, T. Nakanishi, *J. Am. Chem. Soc.* **2006**, *128*, 10024.

[25] S. I. Yang, J. Seth, J. P. Strachan, S. Gentemann, D. Kim, D. Holten, J. S. Lindsey, D. F. Bocian, *J. Porphyrins Phthalocyanines* **1999**, *3*, 117.

[26] **MgCl−P3** is originally non-emissive. The blue-shift in its emission spectrum is in accord with the increase in the intensity of the maximum absorption band at 550 nm seen upon the formation of **MgCl−P3**.

[27] a) A. C. Benniston, G. Copley, H. Lemmetyinen, N. V. Tkachenko, *Eur. J. Org. Chem.* **2010**, 2867; b) G. Duvanel, N. Banerji, E. Vauthey, *J. Phys. Chem. A* **2007**, *111*, 5361; c) H. L. Kee, C. Kirmaier, L. Yu, P. Thamyongkit, W. J. Youngblood, M. E. Calder, L. Ramos, B. C. Noll, D. F. Bocian, W. R. Scheidt, R. R. Birge, J. S. Lindsey, D. Holten, *J. Phys. Chem. B* **2005**, *109*, 20433.

[28] S. Hattori, K. Ohkubo, Y. Urano, H, Sunahara, T. Nagano, Y. Wada, N. V. Tkachenko, H. Lemmetyinen, S. Fukuzumi, *J. Phys. Chem. B* **2005**, *109*, 15368.

[29] a) C. A. Wijesinghe, M. E. El-Khouly, N. K. Subbaiyan, M. Supur, M. E. Zandler, K. Ohkubo, S. Fukuzumi, F. D′Souza, *Chem. Eur. J.* **2011**, *17*, 3147; b) J. Y. Liu, M. E. El-Khouly, S. Fukuzumi, D. K. P. Ng, *Chem. Asian J.* **2011**, *6*, 174; c) M. Galletta, S. Campagna, M. Quesada, G. Ulrich, R. Ziessel, *Chem. Commun.* **2005**, 4222; d) M. Galletta, F. Puntoriero, S. Campagna, C. Chiorboli, M. Quesada, S. Goeb, R. Ziessel, *J. Phys. Chem. A* **2006**, *110*, 4348.

[30] The UV/Vis absorption spectrum of the one-electron-oxidized **MgCl−P1** species is shown in the Supporting Information, Figure S4. The temporal spectroscopic behavior of the charged species upon excitation has previously been observed in push–pull BODIPY molecules; see reference [27a].

[31] This method yields the evolution-associated difference spectra and the spectra of the individual excited-state species, together with their respective rate constants; see: a) I. H. M. van Stokkum, R. H. Lozier, *J. Phys. Chem. B* **2002**, *106*, 3477; b) C. Hippius, I. H. M. van Stokkum, E. Zangrando, R. M. Williams, F. Würthner, *J. Phys. Chem. C* **2007**, *111*, 13988.

[32] a) T. Miura, Y. Urano, K. Tanaka, T. Nagano, K. Ohkubo, S. Fukuzumi, *J. Am. Chem. Soc.* **2003**, *125*, 8666; b) T. Ueno, Y. Urano, K. Setsukinai, H. Takakusa, H. Kojima, K. Kikuchi, K. Ohkubo, S. Fukuzumi, T. Nagano, *J. Am. Chem. Soc.* **2004**, *126*, 14079; c) T. Mineno, T. Ueno, Y. Urano, H. Kojima, T. Nagano, *Org. Lett.* **2006**, *8*, 5963; d) T. Matsumoto, Y. Urano, T. Shoda, H. Kojima, T. Nagano, *Org. Lett.* **2007**, *9*, 3375; e) X. Zhang, L. Chi, S. Ji, Y. Wu, P. Song, K. Han, H. Guo, T. D. James, J. Zhao, *J. Am. Chem. Soc.* **2009**, *131*, 17452; f) X. Li, S. Qian, Q. He, B. Yang, J. Li, Y. Hu, *Org. Biomol. Chem.* **2010**, *8*, 3627; g) Y. Wu, H. Guo, X. Zhang, T. D. James, J. Zhao, *Chem. Eur. J.* **2011**, *17*, 7632.

[33] This trend is opposite to what would be expected for a typical acceptor-excited PET system. Therefore, we conclude that an a-PET (a = acceptor) process does not play a significant role in regulating the excited-state behavior in this instance. When trifluoroacetic acid (TFA) was added to a solution of **H−P1** in MeCN, protonation at the one of the nitrogen atoms of the 1,10-phenanthroline unit took place; see: M. Ishida, S. Karasawa, H. Uno, F. Tani, Y. Naruta, *Angew. Chem.* **2010**, *122*, 6042; *Angew. Chem. Int. Ed.* **2010**, *49*, 5906. On the other hand, no enhancement in the emission characteristics of the protonated form of **H−P1** occurred in the visible-light region (see the Supporting Information, Figure S10). This result provides further support for the conclusion that intramolecular PET from the 1,10-phenanthroline moiety to the acceptor fluorophore (dipyrrin; acceptor-excited PET: a-PET) does not occur to an appreciable extent. See: A. P. de Silva, H. Q. N. Gunaratne, T. Gunnlaugsson, A. J. M. Huxley, C. P. McCoy, J. T. Rademacher, T. E. Rice, *Chem. Rev.* **1997**, *97*, 1515.

[34] D. Rehm, A. Weller, *Isr. J. Chem.* **1970**, *10*, 259.

[35] N. M. O′Boyle, A. L. Tenderholt, K. M. Langner, *J. Comput. Chem.* **2008**, *29*, 839.

[36] a) B. K. Kaletaş, H. C. Joshi, G. van der Zwan, M. Fanti, F. Zerbetto, K. Goubitz, L. D. Cola, B. König, R. M. Williams, *J. Phys. Chem. A* **2005**, *109*, 9443; b) G. Zhao, J. Liu, L. Zhou, K. Han, *J. Phys. Chem. B* **2007**, *111*, 8940; c) K. Saita, M. Nakazono, K. Zaitsu, S. Nanbu, H. Sekiya, *J. Phys. Chem. A* **2009**, *113*, 8213.

[37] X. Zhang, Y. Wu, S. Ji, H. Guo, P. Song, K. Han, W. Wu, W. Wu, T. D. James, J. Zhao, *J. Org. Chem.* **2010**, *75*, 2578.

[38] The fluorescence efficiency of **MgCl−P*n*** is not thought to be regulated exclusively by d-PET processes. Support for this conclusion comes from the realization that the overall fluorescence of all of the Mg complexes is still weak. The fluorescent spectra of both **H−P*n*** and **MgCl−P*n*** at various temperatures reveal a gradual enhancement in emission intensity as the temperature is lowered (see the Supporting Information, Figure S16). On the other hand, photographs of frozen solutions of **H−P1** and **MgCl−P1** in MeCN revealed bright-orange and red emissions, respectively. Thus, we considered it likely that the flexible nature of macrocycles of **H−P*n***, although favoring the complexation of Mg^{2+} ions, also contributes to effective internal-conversion processes that serve to quench the emission.

[39] a) P. Carol, S. Sreejith, A. Ajayaghosh, *Chem. Asian J.* **2007**, *2*, 338; b) K. Kiyose, H. Kojima, T. Nagano, *Chem. Asian J.* **2008**, *3*, 506; c) S. A. Hilderbrand, R. Weissleder, *Curr. Opin. Chem. Biol.* **2010**, *14*, 71.

[40] a) T. Rohand, E. Dolusic, T. H. Ngo, W. Maes, W. Dehaen, *ARKIVOC* **2007**, Part 10, 307; b) Y. Mizuno, T. Aida, K. Yamaguchi, *J. Am. Chem. Soc.* **2000**, *122*, 5278.

[41] O. S. Finikova, T. Troxler, A. Senes, W. F. DeGrado, R. M. Hochstrasser, S. A. Vinogradov, *J. Phys. Chem. A* **2007**, *111*, 6977.

[42] K. A. Connors, *Binding Constants*, J. Wiley, New York, **1987**.

[43] CrystalStructure 3.8.1: Crystal Structure Analysis Package, Rigaku and Rigaku/MSC (2000–2003). 9009 New Trails Dr. The Woodlands TX 77381 USA.

[44] M. J. Frisch, G. W. Trucks, H. B. Schlegel, G. E. Scuseria, M. A. Robb, J. R. Cheeseman, J. A. Montgomery, Jr., T. Vreven, K. N. Kudin, J. C. Burant, J. M. Millam, S. S. Iyengar, J. Tomasi, V. Barone, B. Mennucci, M. Cossi, G. Scalmani, N. Rega, G. A. Petersson, H. Nakatsuji, M. Hada, M. Ehara, K. Toyota, R. Fukuda, J. Hasegawa, M. Ishida, T. Nakajima, Y. Honda, O. Kitao, H. Nakai, M. Klene, X. Li, J. E. Knox, H. P. Hratchian, J. B. Cross, V. Bakken, C. Adamo, J. Jaramillo, R. Gomperts, R. E. Stratmann, O. Yazyev, A. J. Austin, R. Cammi, C. Pomelli, J. W. Ochterski, P. Y. Ayala, K. Morokuma, G. A. Voth, P. Salvador, J. J. Dannenberg, V. G. Zakrzewski, S. Dapprich, A. D. Daniels, M. C. Strain, O. Farkas, D. K. Malick, A. D. Rabuck, K. Raghavachari, J. B. Foresman, J. V. Ortiz, Q. Cui, A. G. Baboul, S. Clifford, J. Cioslowski, B. B. Stefanov, G. Liu, A. Liashenko, P. Piskorz, I. Komaromi, R. L. Martin, D. J. Fox, T. Keith, M. A. Al-Laham, C. Y. Peng, A. Nanayakkara, M. Challacombe, P. M. W. Gill, B. Johnson, W. Chen, M. W. Wong, C. Gonzalez, J. A. Pople, Gaussian, Inc., Wallingford CT, **2004**.

[45] a) A. D. Becke, *Phys. Rev. A* **1988**, *38*, 3098; b) C. Lee, W. Yang, R. G. Parr, *Phys. Rev. B* **1988**, *37*, 785; c) A. D. Becke, *J. Chem. Phys.* **1993**, *98*, 5648.

Received: May 22, 2012

Porphyrinoids

M. Ishida, J. M. Lim, B. S. Lee, F. Tani, J. L. Sessler, D. Kim,* Y. Naruta** .... ▮▮▮▮–▮▮▮▮

Photophysical Analysis of 1,10-Phenanthroline-Embedded Porphyrin Analogues and Their Magnesium(II) Complexes

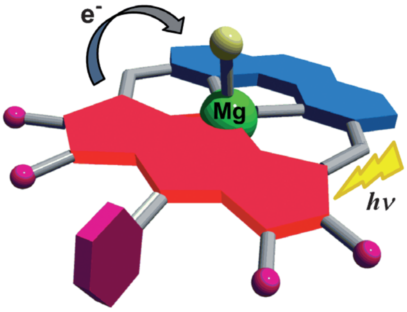

Anything can H-P*n*: A new series of tetraaza porphyrin analogues (**H–P*n***: $n=1$–4) containing a dipyrrin subunit and an embedded 1,10-phenanthroline subunit have been developed as Mg^{2+}-responsive fluorescent sensors. Upon complexation with Mg^{2+} ions, a structure-dependent emission enhancement is seen that is partially governed by donor-excited photoinduced electron-transfer (d-PET) events.